Cation, Vacancy, and Spin Ordered 15R-Superstructures in Sr(Cr1-xFex)O3-y (0.4 x 0.6) Perovskites

Cite as:
Arévalo-lópez, A. M., Sher, F., Farnham, J., Watson, A. J., & Attfield, J. P. (2013). Cation, Vacancy, and Spin Ordered 15R-Superstructures in $Sr(Cr_{1-x}Fe_x)O_{3-y}$ ($0.4 \leq x \leq 0.6$) Perovskites. *Chemistry of Materials*, 25(11), 2346-2351.

Manuscript received: 02/04/2013; Accepted: 22/05/2013; Article published: 30/05/2013

Cation, Vacancy, and Spin Ordered 15R-Superstructures in $Sr(Cr_{1-x}Fe_x)O_{3-y}$ ($0.4 \leq x \leq 0.6$) Perovskites**

Angel M. Arévalo-López,[1] Falak Sher,[2] James Farnham,[1] Adam J. Watson[1] and J. Paul Attfield[1,*]

[1]EaStCHEM, School of Chemistry and Centre for Science at Extreme Conditions (CSEC), Joseph Black Building, University of Edinburgh, West Mains Road, Edinburgh, EH9 3JJ, UK.

[2]School of Science and Engineering, Lahore University of Management Sciences (LUMS), Pakistan.

[*]Corresponding author; e-mail; j.p.attfield@ed.ac.uk

[**]We acknowledge support from EPSRC, STFC, the Leverhulme Trust, the Royal Society of Edinburgh, and the Royal Society. We thank Drs. K. Knight (ISIS) and Chiu C Tang (Diamond) for assistance with diffraction measurements.

Graphical abstract:

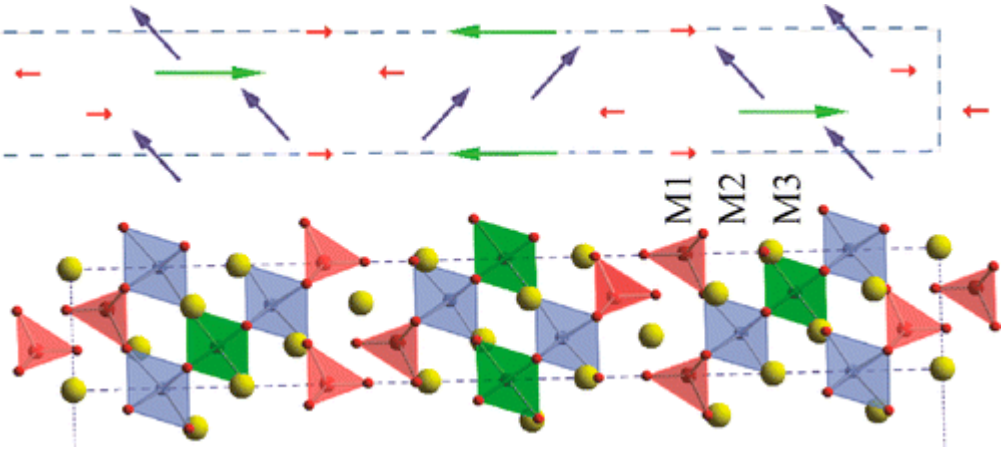

Keywords:
perovskite oxides; magnetic structure; solid oxide fuel cells

Abstract

15-layer rhombohedral (15R) $SrCrO_{2.8}$-type superstructures have been discovered in $Sr(Cr_{1-x}Fe_x)O_{3-y}$ perovskites ($0.4 \leq x \leq 0.6$; space group $R\bar{3}m$; $a \approx 5.56$ and $c \approx 34.6$ Å). Cr/Fe cations are segregated between layers of tetrahedrally and octahedrally coordinated sites. The 15R-$Sr(Cr_{1-x}Fe_x)O_{3-y}$ materials are semiconducting and order ferrimagnetically below 225–342 K. The magnetic structure of an $x = 0.5$ sample shows spin canting consistent with a simple spin disorder model. Samples with $x \geq 0.7$ have a disordered cubic perovskite structure, and we propose that locally reconstructed (111) planes like those in the 15R materials facilitate oxide ion migration in Cr-based perovskite mixed conductors used in solid oxide fuel cells.

Introduction

Perovskites are fundamentally and technologically important because of the wide variety of phenomena they show, e.g. high-T_C superconductivity, colossal magnetoresistance (CMR), mixed electron and oxygen ion conductivity, and rich magnetic behaviors. These properties are often determined by cation or anion ordering in perovskite superstructures. For instance CMR in Sr_2FeMoO_6 depends on the long-range Fe/Mo ordering in the B-cation sublattice.[1] Anion vacancies promote ionic conductivity, and when variable cation oxidation states provide electronic conductivity, then useful mixed conductors for solid-oxide fuel cells (SOFC) anodes may result, e.g. $(La_{1-x}Sr_x)(Cr_{1-y}M_y)O_{3-\delta}$ (M = Mn, Fe, Co, Ni).[2] Further structural variety results from mixed cubic and hexagonal stacking sequences, for example, 6H, 8H, 10H, and 15R, hexagonal $BaMnO_{3-\delta}$ polytypes show a correlation between the stacking sequence and magnetic ordering transition temperature.[3]

$SrCr_{1-x}Fe_xO_{3-y}$ perovskites are of potential interest as mixed conductors or as possible CMR analogues of Sr_2FeMoO_6 for $x = 0.5$. Previous studies have shown that the $SrCr_{1-x}Fe_xO_{3-y}$ system is complex. Gibb and Matsuo initially identified three polytypes depending on synthesis conditions: a cubic perovskite, a 15R (15-layer rhombohedral) material with oxygen contents 2.68–2.78, and an orthorhombic phase.[4] Structural models were not obtained for the latter two phases, but subsequent Mössbauer and EXAFS spectroscopy studies showed that Fe^{3+} is present in several oxygen coordinations.[5, 6] A recent neutron pair-distribution function study of an $x = 0.75$ cubic sample revealed that the local structure is described well in a brownmillerite-type framework.[7]

During a recent proof-of-concept demonstration of "hard–soft" chemistry, a new $SrCrO_{2.8}$ phase was prepared by "soft" low temperature reduction of the perovskite $SrCrO_3$, which had been synthesized under "hard" high pressure and temperature conditions.[8] $SrCrO_{2.8}$ was discovered to have a 15R superstructure with an all cubic $(ccc'cc)_3$ stacking sequence, where c' is an oxygen deficient layer, like that in $Ba_5MnNa_2V_2O_{13}$,[9] rather than a mixed cubic (c) and hexagonal (h) sequence as reported in other 15R materials; $(hhchh)_3$ e.g. in $BaMnO_3$[3] or $(chchc)_3$ e.g. in $SrMn_{1-x}Fe_xO_{3-\delta}$.[10] Attempts to stabilize $SrCrO_{2.8}$ through chemical substitutions in ref 8 led to the discovery that the 15R $SrCr_{1-x}Fe_xO_{3-y}$ phase reported earlier by Gibb and Matsuo[4] has the same structure

type. We have thus reinvestigated these materials, and we report here the composition range, structural results, and magnetic and electronic conducting properties for $SrCrO_{2.8}$-type 15R-$SrCr_{1-x}Fe_xO_3$ perovskites. The concentration of defects in reconstructed (111) planes may be important to oxide ion migration in Cr-based perovskite mixed conductors used in SOFC anodes.

Experimental Section

Polycrystalline samples of nominal compositions $Sr(Cr_{1-x}Fe_x)O_{3-y}$ ($0.2 \leq x \leq 0.8$) were prepared by solid-state reaction. Stoichiometric mixtures of $SrCO_3$, Fe_2O_3, and Cr_2O_3 (Sigma Aldrich, ≥3N) were ground together, pelletized, heated at 1200 °C for 24 h under a flowing argon atmosphere, and quenched in liquid nitrogen. The quench was needed to minimize the formation of $Sr_3Cr_2O_8$ and $SrCrO_4$ secondary phases.

Powder X-ray diffraction characterization was performed with a Bruker AXS D2 Phaser instrument equipped with Cu Kα radiation. The $x = 0.5$ sample was studied further using synchrotron X-ray and neutron diffraction. Room temperature synchrotron data were recorded at the I11 beamline of the Diamond Light Source, with wavelength $\lambda = 0.8273$ Å.[11] Time-of-flight neutron powder diffraction patterns were collected at instrument HRPD on the ISIS spallation source in the 4–400 K temperature range in 10 K intervals and normalized with MantidPlot.[12] Rietveld and magnetic symmetry analyses were performed using Fullprof Suite including BASIREPS for magnetic symmetry analysis.[13, 14]

Magnetic properties were measured with a commercial SQUID magnetometer (MPMS, Quantum Design) under zero field cooled (ZFC) and field cooled (FC) conditions in the 2–400 K temperature range with a 0.5 T applied field. Four-point resistivity measurements were performed in a closed-cycle cryostat.

Results

Figure 1 shows the powder X-ray data for samples of nominal composition $SrCr_{1-x}Fe_xO_{3-y}$ ($0.2 \leq x \leq 0.8$). 15R-$SrCr_{1-x}Fe_xO_{3-y}$ solid solutions are observed in the $0.4 \leq x \leq 0.6$ range and give rise to a splitting of the intense diffraction peak at $2\theta \approx 32°$. A mixture of the 15R-$SrCr_{1-x}Fe_xO_{3-y}$ phase and $Sr_3Cr_2O_8$ is observed in $x = 0.2$ and 0.3 samples, and a trace of $Sr_3Cr_2O_8$ is observed for $x = 0.4$, perhaps due to slight decomposition during the quench from 1200 °C. However, the evolution of the 15R-$SrCr_{1-x}Fe_xO_{3-y}$ cell parameters and volume for $0.4 \leq x \leq 0.6$ samples is consistent with a solid solution across this range under the present synthesis conditions. The 15R superstructure is not observed in samples with $x \geq 0.7$, and a disordered *Pm3m* cubic perovskite structure with a single peak at $2\theta \approx 32°$ is obtained, as reported for $SrFe_{0.75}Cr_{0.25}O_{3-y}$.[7] Cell parameters of the 15R phase at 300 K were obtained by fitting a $SrCrO_{2.8}$-type model in space group $R\bar{3}m$ and are shown in Table 1. The increase in lattice parameters and volume with x is consistent with the larger size of Fe ions compared to Cr.[15]

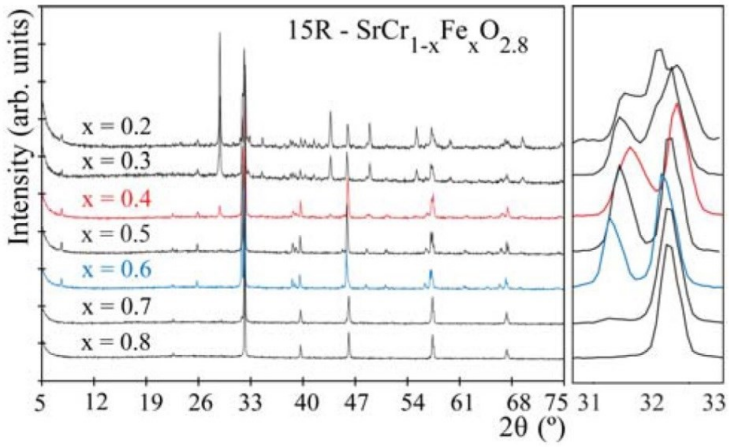

Figure 1. Powder X-ray diffraction data for $Sr(Cr_{1-x}Fe_x)O_{3-y}$ ($0.2 \leq x \leq 0.8$) compositions with an expansion of the intense peak at 31–33°. Additional peaks from $Sr_3Cr_2O_8$ are observed at x = 0.2, 0.3, and 0.4.

The magnetic susceptibilities for x = 0.4, 0.5, and 0.6 samples measured on warming in a 0.5 T magnetic field for ZFC and FC conditions are shown in Figure 2. Ferro- or ferrimagnetic transitions are observed with Curie temperatures that increase with x, as shown in Table 1. A small divergence between ZFC and FC susceptibilities is observed below T_C for all samples. The inset of Figure 2 shows the inverse susceptibility vs temperature with a Curie–Weiss fit to high temperature data. The positive Weiss temperatures θ are indicative of dominant ferromagnetic interactions, and the paramagnetic moments of 3.3–3.7 μ_B are consistent with high spin Fe and Cr ions, although the observed temperature interval above T_C is not sufficient to provide reliable moments.

Saturated moments of 0.2–0.3 μ_B per M (=Cr/Fe) site observed in magnetization-field hysteresis loops (Figure 3) show that the spin order is ferri- or weakly ferromagnetic. Coercive fields of up to 0.14 T for the x = 0.6 sample show that the uniaxial 15R-$SrCrO_{2.8}$-type structure creates significant magnetic anisotropy.

Table 1. Parameters Derived from X-ray Diffraction, Magnetization, and Resistivity Measurements on 15R-$Sr(Cr_{1-x}Fe_x)O_{3-y}$ Samples with x = 0.4, 0.5, and 0.6[a].

x	**0.4**	**0.5**	**0.6**
a (Å)	5.5519(4)	5.5573 (2)	5.5671(2)
c (Å)	34.515(3)	34.586(1)	34.680(1)
V (Å^3)	921.344(4)	925.04(6)	930.824(3)
T_C (K)	225(1)	260(1)	342(1)
θ (K)	245(1)	247(1)	303(1)
μ_{eff} (μ_B)	3.37(3)	3.33(2)	3.66(3)
μ_{sat} (μ_B)	0.271(1)	0.256(2)	0.191(1)
H_c (T)	0.050(1)	0.025(1)	0.140(1)
E_a (eV)	0.207(1)	0.136(1)	0.191(1)

[a]Fitting errors are shown in parentheses.

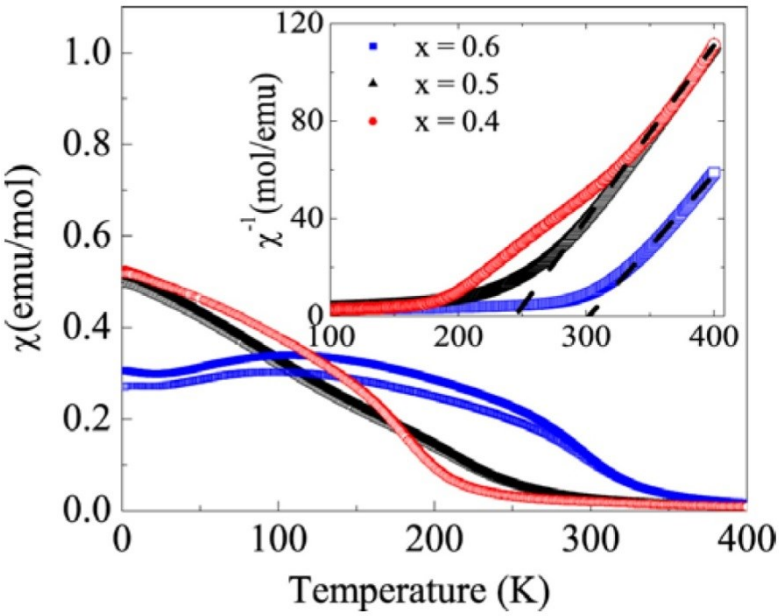

Figure 2. ZFC (open points) and FC (closed points) magnetic susceptibilities for 15R-$SrCr_{1-x}Fe_xO_{3-y}$ ($0.4 \leq x \leq 0.6$) samples. The inset shows inverse ZFC data with Curie–Weiss fits at high temperatures (fits for $x = 0.4$ and 0.5 overlap).

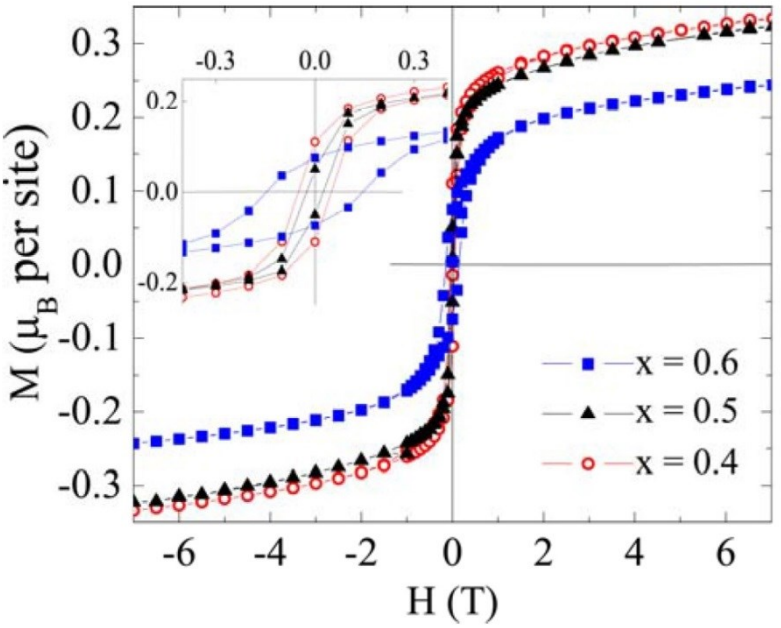

Figure 3. Magnetisation-field loops at 4 K for the 15R-$SrCr_{1-x}Fe_xO_{3-y}$ ($0.4 \leq x \leq 0.6$) samples, with low field variations shown in the inset.

15R-$SrCr_{1-x}Fe_xO_{3-y}$ materials show moderate electrical resistivities of 0.1–0.3 Ωm at 300 K. Variable temperature measurements show semiconducting behavior for ceramic pellets of x = 0.4, 0.5, and 0.6 samples (Figure 4). The sample resistances were too high to be measured accurately below 120 K. Resistivities in the magnetically ordered regimes show Arrhenius behavior (but with experimental artifacts for the x = 0.6 sample), and the fitted band gap energies are in the range 140–210 meV as displayed in Table 1. The resistivity of the x = 0.4 sample deviates from the fitted Arrhenius law toward lower values as temperature increases above T_C = 225 K, showing that the predominantly antiferromagnetic order lowers electron mobility. There are insufficient data above T_C to verify this change for the x = 0.5 sample, and all measured x = 0.6 resistivities are in the magnetically ordered regime.

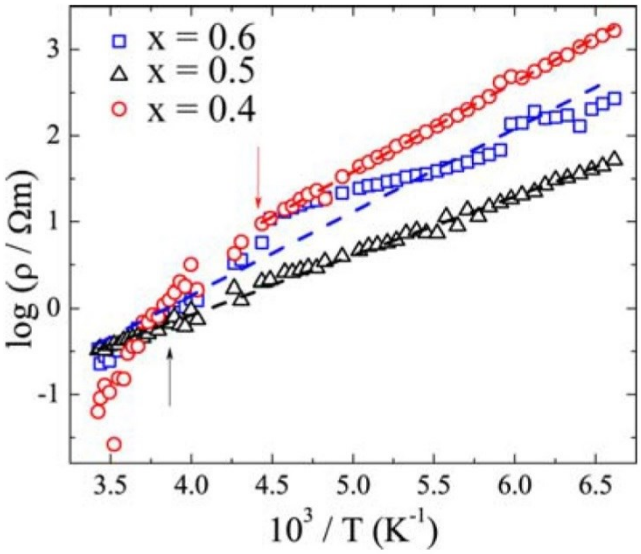

Figure 4. Arrhenius plot of electronic resistivities for the 15R-$SrCr_{1-x}Fe_xO_{3-y}$ (x= 0.4, 0.5, and 0.6) samples, with arrows marking T_C for the former two samples.

Figure 5 shows the combined synchrotron and neutron Rietveld refinement plot of the 15R-$SrCrO_{2.8}$-type model for $Sr(Cr_{0.5}Fe_{0.5})O_{3-y}$.[8] The final structural parameters from the combined 300 K synchrotron and neutron refinement and from a fit to HRPD neutron data at 4 K are summarized in Table 2. The 15R-$Sr(Cr_{1-x}Fe_x)O_{2.8}$ model consists of cubic (c) SrO_3 layers and an SrO_2 oxygen deficient (c') layer stacked along the cubic perovskite [111] direction in a $(ccc'cc)_3$sequence. This results in double layers of MO_4 tetrahedra between three perovskite blocks (Figure 6b).

Sr2 and O2 sites in the c' layer were initially refined on their ideal 3a and 6c sites, but anomalous thermal displacement factors were observed, with a large ab-plane amplitude from anisotropic refinement. This evidence some local disorder in the oxygen-deficient c' planes, so these atoms were respectively displaced

from ideal positions to split 18*f* and 18*h* sites as shown in Table 2. The split site refinement gives a range of Sr2–O2 distances ~2.78–3.85 Å around the 3.23 Å value for the ideal sites. Such disorder in oxygen deficient layers is observed in other complex perovskites, e.g. $Ba_7Y_2Mn_3Ti_2O_{20}$.[16] No significant deviation in oxygen content was obtained by varying the O site occupancies, so the final refined model has the ideal $Sr(Cr_{0.5}Fe_{0.5})O_{2.8}$composition. Refinement of Cr/Fe occupancies at the transition metal (M) sites showed that the tetrahedral M1 sites are chromium rich (83% Cr), whereas the M2 octahedra in the adjacent layers are iron rich (81% Fe) and the central M3 octahedra are close to a statistical 50% Cr/50% Fe ratio.

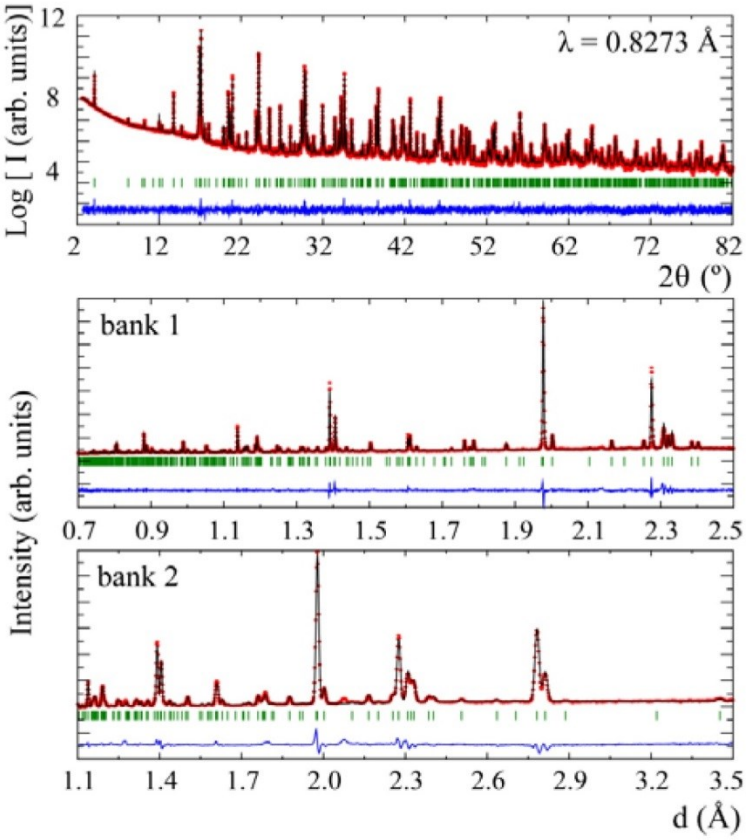

Figure 5. Combined Rietveld fit to 300 K synchrotron X-ray (top; intensities plotted on a log scale) and HRPD neutron (middle; bank 1 - 2θ = 168.33°; bottom bank 2 - 2θ = 90°) powder diffraction for 15R-$Sr(Cr_{0.5}Fe_{0.5})O_{3-y}$.

Bond valence sums (BVS)[17] for the three M cation sites were calculated from the 300 K M-O bond distances using a standard interpolation method[18] and bond valence parameters for Cr^{3+}, Cr^{4+}, Fe^{3+}, and Fe^{4+}, as shown in Table 3. These demonstrate that the tetrahedrally coordinated, Cr-rich M1 site has +4 cations, while the octahedral M2 and M3 cations are close to the +3 state. The M1, M2, and M3 site cations have +4, +3.5, and +3 charges in the 15-$SrCrO_{2.8}$aristotype, so the present results for $SrCr_{1-x}Fe_xO_{3-y}$ show that the M2 sites are

reduced in line with the reported oxygen content range of 2.68–2.78.[4] A value of 2.7 is expected for ideal M1, M2, and M3 charges of +4, +3, and +3, hence the reported limits are in excellent agreement with a stability range y = 0.2–0.3 for the 15R-$SrCr_{1-x}Fe_xO_{3-y}$ structure.

Table 2. Lattice Parameters, Atomic Coordinates, Isotropic Thermal Displacement Parameters and Site Occupancies from Neutron Refinements of 15R-$Sr(Cr_{0.5}Fe_{0.5})O_{2.8}$ at 300 K (Upper Values) and 4 K (Lower Values) in Space Group$R\bar{3}m$[a,c].

a **(Å)**		***c*** **(Å)**		**volume (Å^3)**	
5.56120(1)		34.6193(1)		927.227(2)	
5.54838(3)		34.5263(5)		920.48(2)	
	x	***y***	***z***	U_{iso} **(Å^2)**	**occ**[b]
Sr1	0	0	0.40859(5) 0.40854(2)	0.011(1) 0.0033(1)	1
Sr2	0.0518(8) 0.0066(3)	0	0	0.009 (1) 0.0070(5)	0.1667
Sr3	0	0	0.19417(5) 0.19385(2)	0.009(1) 0.003(2)	1
M1	0	0	0.29156(7) 0.29215(3)	0.0053(1) 0.0004(7)	0.83(1)/ 0.17
M2	0	0	0.10349(6)0.10305(2)	0.0037(2) 0.0004	0.19(1)/ 0.81
M3	0	0	0.5	0.0048(2) 0.0004	0.43(5)/ 0.57
O1	0.5008(1) 0.4997(7)	0.4992 0.5003	0.3954(1) 0.3956(1)	0.0230(3) 0.0053(7)	1
O2	0.039(1) 0.045(2)	0.078 0.090	0.3384(3) 0.3394(2)	0.025(3) 0.0028(4)	0.3333
O3	0.5013(1) 0.4983(9)	0.4987 0.5017	0.2009(1) 0.2010(1)	0.0072(3) 0.010(8)	1

[a]Residuals are R_{wp} = 0.064, χ^2 = 3.29 (300 K); R_{wp} = 0.082, χ^2 = 3.48 (4 K). Refined magnetic moments at 4 K for M1, M2, and M3 are respectively 1.0(1), 3.0(2), and 4.4(3)μ_B.

[b]Cr/Fe occupancies shown for M sites were refined at 300 K.

[c]Estimated standard deviations of independent variables are shown in parentheses.

Magnetic neutron diffraction peaks are observed in the low temperature HRPD patterns of $Sr(Cr_{0.5}Fe_{0.5})O_{3-y}$. These peaks are indexed by two magnetic propagation vectors, k_1 = (0 0 0) and k_2 = (0 0 3/2). The intensities of the k_1 and k_2 reflection sets evolve similarly with temperature and both vanish at ≈260 K, implying that their irreducible representations (irreps) are strongly coupled.[19] The possible irreps and basis vectors for k_1= (0, 0, 0) and k_2= (0, 0, 3/2) propagation vectors applied to the $R\bar{3}m$ space group are shown in Table 4.

A good fit to the magnetic intensities (Figure 6a) is obtained using basis vector $\Psi_1(\Gamma_2,k_2)$ for all three cation sites and an additional $\Psi_5(\Gamma_6,k_1)$ component for M2 spins only. Ψ_1 describes an antiferromagnetic ordering of moments along the *z*-axis, whereas Ψ_5 defines a ferromagnetic arrangement in the *ab*-plane. Components in the *ab*-plane for M1 and M3 converged to zero when refined. The evolution with temperature of the refined magnetic moments for the three sites is shown in Figure 7. The fit of a critical law $m(T) = m(0)[1–(T/T_N)]^{\beta}$ to the magnetic moments in the 130–260 K range gives $T_N = 263(2)$ K and $\beta = 0.34(3)$. The exponent agrees well with the theoretical value of 0.36 for the three-dimensional Heisenberg model.[20]

Table 3. Bond Distances and Bond Valence Sums for the M Sites for 15R-$Sr(Cr_{0.5}Fe_{0.5})O_{2.8}$ at 300 K.

	bond length (Å)		**bond length (Å)**
M1–O1 (x 3)	1.760(3)	<Sr1–O>	2.663(3)
M1–O2 (x 1)	1.666(4)	<Sr2–O1>	2.69(2)
M2–O1 (x 3)	2.147(1)	<Sr2–O2>	2.97(4)
M2–O3 (x 3)	1.882(1)	<Sr2–O>	2.83(1)
M3–O3 (x 6)	2.006(2)	Sr3–O1 (x 3)	3.119(3)
Sr1–O1 (x 6)	2.818(2)	Sr3–O3 (x 3)	2.666(2)
Sr1–O2 (x3)	2.461(4)	Sr3–O3 (x 6)	2.790(2)
Sr1–O3 (x 3)	2.555(2)	<Sr3–O>	2.841(3)

BVS[a]	**Cr**	**Fe**	**average**
M1	4.04	4.09	4.05
M2	2.90	3.18	3.13
M3	2.78	3.07	2.94

[a]BVS's are shown for M site occupancy by Cr, by Fe, and by the weighted average Cr/Fe content using occupancies from Table 2.

Table 4. Irreducible Representations and Basis Vectors of Magnetic Moments for k_1=(0, 0, 0) and k_2= (0, 0, 3/2) Propagation Vectors Applied to M1, M2, and M3 Cations at (0,0,*z*) and (0,0,–*z*) in Space Group $R\bar{3}m$.

		$\mathbf{m}_x, \mathbf{m}_y, \mathbf{m}_z$	
irreps	**basis vectors**	**(0,0,*z*)**	**(0,0,–*z*)**
Γ_2	Ψ_1	0, 0, 1	0, 0, −1
Γ_3	Ψ_2	0, 0, 1	0, 0, 1
Γ_5	Ψ_3	$3/2 – \sqrt{3}/2i$, $-\sqrt{3}\,i$, 0	$–3/2 + \sqrt{3}/2i$, $\sqrt{3}i$, 0
	Ψ_4	$\sqrt{3}i$, $–3/2 + \sqrt{3}/2i$, 0	$-\sqrt{3}\,i$, $3/2 – \sqrt{3}/2i$, 0
Γ_6	Ψ_5	$3/2 – \sqrt{3}/2i$, $-\sqrt{3}i$, 0	$3/2 – \sqrt{3}/2i$, $-\sqrt{3}\,i$, 0
	Ψ_6	$–\sqrt{3}i$, $3/2 – \sqrt{3}/2i$, 0	$–\sqrt{3}i$, $3/2 – \sqrt{3}/2i$, 0

Discussion

The present results confirm that the 15R phase reported in the $SrCr_{1-x}Fe_xO_{3-y}$ system[5, 6] is isostructural with $SrCrO_{2.8}$, recently discovered through hard–soft reduction of $SrCrO_3$.[8] This has an unconventional structure for a reduced cubic-type $AMO_{3-\delta}$ perovskite as the oxygen vacancies are formed in (111) planes, rather than the normal mechanism of (100)-plane deficiency found e.g. in $CaFeO_{2.5}$ brownmillerite. The $SrCrO_{2.8}$-type structure is also unusual because oxide vacancies are formed only in every fifth (111)-plane, giving rise to a

large-scale superstructure of the cubic perovskite arrangement with $c \approx 34.6$ Å. This is characterized by $(ccc'cc)_3$ stacking of AMO_3 perovskite layers, with oxide reconstruction and vacancy order in thec' (111) planes, that gives rise to tetrahedral coordination of M cations in the adjacent planes. The double tetrahedral layers are separated by triple layers of unreconstructed cubic perovskite with octahedral M-coordination. The ideal stoichiometry for this superstructure is represented by the aristotype material $SrCrO_{2.8}$ ($Sr_5Cr_5O_{14}$).

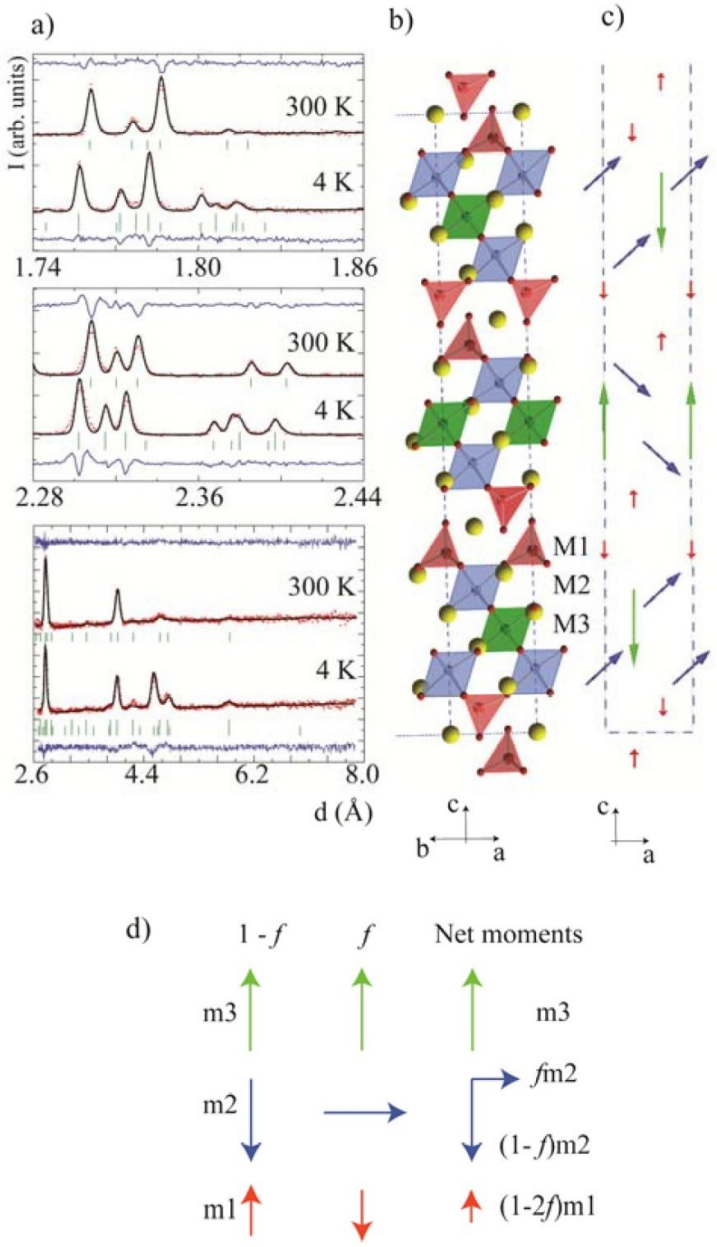

Figure 6. a) Selected regions of 300 and 4 K neutron Rietveld refinements for 15R-$Sr(Cr_{0.5}Fe_{0.5})O_{2.8}$ showing magnetic reflections at 4 K. b) 15R crystal structure of $SrCr_{0.5}Fe_{0.5}O_{2.8}$. c) Magnetic structure at 4 K showing half the magnetic supercell. d) Schematic disorder model for the canting of moments, as described in the text.

The 15R-$SrCrO_{2.8}$-type structure can tolerate small excess oxygen deficiencies. Oxygen vacancies were reported at the O3-sites, using the structural setting of Table 2, for $BaMn_{0.2}Na_{0.4}V_{0.4}O_{2.6}$ ($Ba_5MnNa_2V_2O_{13}$) which was the first material discovered to have this structure type. Hence it is notable that reduced $SrCrO_{2.8}$ types have both well-ordered (reconstructed) and disordered planes of oxide vacancies. Oxygen-vacancy order can vary markedly between similar systems, for example, in reduced stoichiometric $A_2MX_{3.5}$ layered materials vacancies are ordered in $MX_{1.5}$ perovskite layers of $Nd_4Cu_2O_7$[21] but are disordered in $La_4Li_2O_7$.[22] The previous study of $SrCr_{1-x}Fe_xO_{3-y}$ showed that the oxygen content of the 15R phase varies between 2.7 and 2.8.[4] With knowledge of the structure type, this reveals a corresponding variation of the average charge at the M2 sites (which are coordinated by O3) between +3 and +3.5. The lower limit is likely to be achieved by creation of 8.3% vacancies at the O3-sites - these were not evidenced in the present neutron study of an x = 0.5 sample, although the BVS for the M2 site suggests that the oxidation state is lower than 3.5. The most highly charged cations are always found at the tetrahedral M1 sites in 15R-$SrCrO_{2.8}$ types: Cr^{4+}in $SrCrO_{2.8}$, $(Cr/Fe)^{4+}$ in $SrCr_{1-x}Fe_xO_{3-y}$ (as evidenced by the BVS's in Table 3), and V^{5+} in $BaMn_{0.2}Na_{0.4}V_{0.4}O_{2.6}$.

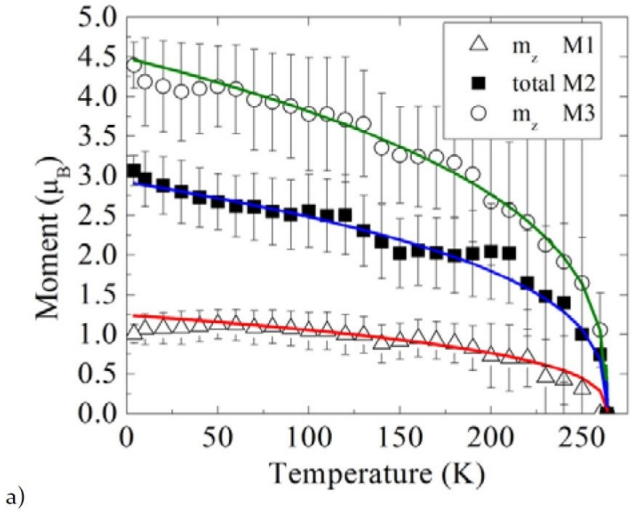

a)

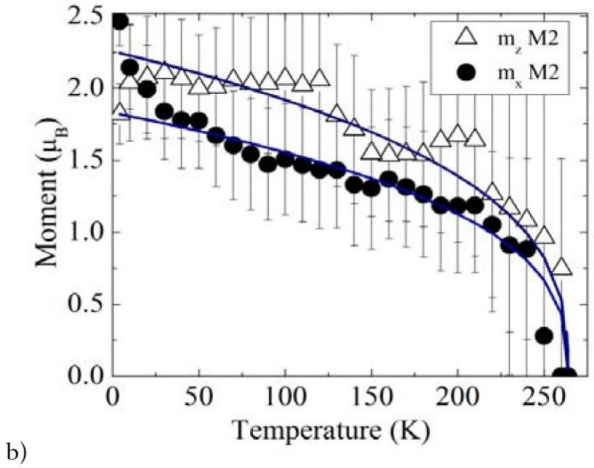

b)

Figure 7. a) Variation of the magnetic moments with temperature, showing critical law fits as described in the text for (a) total moments at each site and (b) m_x and $m_z$components for the M2 site.

The segregation of Cr/Fe over M1 and M2 sites evidenced by the neutron results in Table 3demonstrates that the 15R superstructure is formed at relatively high temperatures, where Cr/Fe-cation mobility is significant. Cr preferentially occupies the M1 sites, in keeping with the relative stabilities of Cr^{4+} and Fe^{4+} under reducing conditions. However, it is surprising that the M2 site which tends to stabilize more highly charged cations than M3 is predominantly occupied by Fe, while M3 has a near-statistical Cr/Fe mixture.

The $x \approx 0.4$ lower limit found for the $SrCrO_{2.8}$-type phase in this study of the $SrCr_{1-x}Fe_xO_{3-y}$system is a solid-solubility boundary, as coexistence with the ternary $Sr_3Cr_2O_8$ phase is observed for lower x compositions. High pressure synthesis, perhaps with subsequent low temperature reduction (hard–soft synthesis), might be used to extend the lower limit of the 15R phase down to the previously reported $x = 0$ composition. The 15R structure changes to a disordered cubic perovskite at an $x \approx 0.7$ upper limit, without the apparent coexistence of the two phases. This implies that an order–disorder transition exists between the two structures, and hence that the oxygen-deficient double tetrahedral layers may be predominant locally extended defects in the disordered materials. This is corroborated by a recent neutron pair-distribution function study of a disordered $x = 0.75$ sample, which reported that the local structure is described by a brownmillerite-type arrangement.[7] The brownmillerite-type has equal amounts of octahedrally and tetrahedrally coordinated Fe cations so it has a similar coordination distribution to the $SrCrO_{2.8}$-type which has 40% tetrahedral and 60% octahedral sites. Further neutron-pdf studies to compare critically the two types as approximants to the local structure of Fe-rich $SrCr_{1-x}Fe_xO_{3-y}$ materials will thus be worthwhile.

Chromium-based perovskites such as $(La_{1-x}Sr_x)(Cr_{1-y}Fe_y)O_{3-\delta}$ have mixed (electronic and ionic) conductivity from variable transition metal valences and oxide vacancies and are used in solid oxide fuel cell (SOFC) anodes.[23] The present $Sr(Cr_{1-x}Fe_x)O_{3-y}$ materials were prepared at high temperature and low oxygen partial pressure conditions similar to those of working SOFC anodes (although the latter are typically exposed to more reducing atmospheres). Hence, the local structures may be similar to those in the 15R- $SrCrO_{2.8}$-type materials. An unusual feature of this structure type is that oxygen vacancies are highly segregated – one-third of the oxides are missing from every fifth cubic (111)-type layer, while the other four layers are pristine. This local concentration of vacancies within the reconstructed c' SrO_2 layers is likely to facilitate oxide ion migration in these planes. Hence, the formation of extended but not long-range-ordered c'-like defect layers may be responsible for the high oxide ion conductivity associated with doped Cr-perovskites.

The 15R-$SrCr_{1-x}Fe_xO_{3-y}$ samples order magnetically with Curie temperatures that increase from 225 to 342 K as x changes from 0.4 to 0.6. These values are comparable to the 272 K magnetic ordering temperature of 15R-$SrCrO_{2.8}$,[8] but a much higher value of 565 K was reported for the disordered cubic $x = 0.75$ sample.[7] Such high spin ordering temperatures are notable given the Cr/Fe disorder present, but similar magnitudes are reported in related cation-disordered perovskites, e.g. up to 480 K in $SrCr_xRu_{1-x}O_3$ perovskites.[24]

The spin order determined from the neutron diffraction study of the $x = 0.5$ sample has two contributions with different propagation vectors, as shown in Figure 6. The m_z components have a simple antiferromagnetic arrangement where m_z-spins in each layer are parallel to each other and antiparallel to those in adjacent layers. This arrangement was observed in 15R-$SrCrO_{2.8}$, and it doubles the *c*-axis periodicity. The second magnetic basis observed in 15R-$Sr(Cr_{0.5}Fe_{0.5})O_{2.8}$ is a ferromagnetic m_x component at M2 sites only which cants the net M2 spins. The low temperature value of $m_x(M2) = 1.8(2)\ \mu_B$ in Figure 7(b) corresponds to a saturated moment of 0.7(2) μ_B per formula unit. This is comparable to values of 0.2–0.3 μ_B taken from the magnetic hysteresis data in Figure 3 and Table 1. The two magnetic modes are strongly coupled and both display the same critical behavior, as shown in Figure 7.

The refined magnetic moments at 4 K for M1, M2, and M3 sites are respectively 1.0(1), 3.0(2), and 4.4(3)μ_B, whereas predicted values based on high-spin-only moments and the ideal M site oxidation states for the $SrCrO_{2.8}$ model are m1 = 2.3, m2 = 4.1, and m3 = 4.1 μ_B. Hence some frustration or disorder of M1 and M2 moments is evident, while the M3 spins are well-ordered. The moment reductions and canting of M2 moments are consistent with a simple disorder model where a fraction *f* of M1 spins are antiparallel to the 1–*f* majority, as shown in Figure6(d). This probably results from different exchange interactions between Cr and Fe ions at the M1 sites. Reversing the direction of an M1 spin frustrates symmetric (Heisenberg) antiferromagnetic interactions of a neighboring M2 spin with M1 and M3 so it adopts a perpendicular orientation due to weaker antisymmetric (Dzyaloshinskii-Moriya) interactions. Comparing the expected moment components shown in Figure 6(d) to the saturated values from neutron results in Figure 7 gives $m_z(M1) = (1–2f)m1 = 1.0(1)\ \mu_B$, $m_x(M2) = fm2 = 1.8(2)\ \mu_B$, and $m_z(M2) = (1–f)m2 = 2.3(2)\ \mu_B$. Using the above ideal moments of m1 = 2.3 and m2 = 4.1 $\mu_B$gives values of $f = 0.28$, 0.44, and 0.44 from the former three equations. The reasonable agreement between these estimates validates the disorder model.

Conclusions

This study demonstrates that reduced $SrCr_{1-x}Fe_xO_{3-y}$ perovskites in the $0.4 \leq x \leq 0.6$ range adopt the 15R-$SrCrO_{2.8}$-type superstructure with reconstructed oxygen-deficient (111) planes that give rise to tetrahedral coordination of adjacent cations. Fe thus stabilizes this unusual structure type, which required 'hard–soft' synthesis for $SrCrO_{2.8}$. Tetrahedral sites are preferentially occupied by Cr, while Fe occupies octahedral sites in the triple perovskite layers. Materials with $x > 0.7$ are disordered cubic perovskites, and we propose that the same (111) oxygen-deficient planes are the dominant local defect and thus may control oxide ion migration in related Cr-based perovskite mixed conductors used in SOFC anodes.

These 15R materials order magnetically close to room temperature, and the magnetic structure for an $x = 0.5$ sample has both antiferromagnetic and ferromagnetic modes present. Observed reductions and canting of moments are consistent with a simple disorder model that reflects local variations of exchange interactions due to Cr/Fe disorder.

References

[1] Kobayashi, K. I.; Kimora, T.; Sawada, H.; Terakura, K.; Tokura, Y. *Nature* **1998**, 395, 677–680.

[2] Cowin, P. I.; Petit, Ch. T. G.; Lan, R.; Irvine, J. T. S.; Tao, Sh. *Adv. Energy Mater.* **2011**,1, 314– 332.

[3] Adkin, J. J.; Hayward, M. A. *Chem. Mater.* **2007**, 19, 755– 762.

[4] Gibb, T. C.; Matuso, M. *J. Solid State Chem.* **1990**, 86, 167– 174.

[5] Gibb, T. C. *J. Mater. Chem.* **1991**, 1, 23– 28.

[6] Gibb, T. C. *J. Mater. Chem.* **1992**, 2, 57– 64.

[7] Ramezanipour, F.; Greedan, J. E.; Siewenie, J.; Donaberger, R. L.; Turner, S.; Botton, G. A. *Inorg. Chem.* **2012**, 51, 2638– 2644.

[8] Arévalo-López, A. M.; Rodgers, J. A.; Senn, M. S.; Sher, F.; Farnham, J.; Gibbs, W.; Attfield, J. P. *Angew. Chem., Int. Ed.* **2012**, 51, 10791– 10794.

[9] Bendraoua, A.; Quarez, E.; Abraham, F.; Mentre, O. *J. Solid State Chem.* **2004**, 177, 1416–1424.

[10] Cussen, E. J.; Sloan, J.; Vente, J. F.; Battle, P. D.; Gibb, T. C. *Inorg. Chem.* **1998**, 37,6071– 6077.

[11] Thompson, S. P.; Parker, J. E.; Potter, J.; Hill, T. P.; Birt, A.; Cobb, T. M.; Yuan, F.; Tang,C. C. *Rev. Sci. Instrum.* **2009**, 80, 075107.

[12] http://www.mantidproject.org/Main_Page (accessed May 19, 2013).

[13] Rodriguez-Carvajal, J. *Phys. B* **1993**, 192, 55– 69.

[14] Ritter, C. *Solid State Phenom.* **2011**, 170, 263– 269.

[15] Shannon, R. D. *Acta Crystallogr.* **1976**, A32, 751– 767.

[16] Kuang, X.; Allix, M.; Ibberson, R. M.; Claridge, J. B.; Niu, H.; Rosseinsky, M. *Chem. Mater.***2007**, 19, 2884– 2893.

[17] Brown, I. D.; Altermatt, D. *Acta Crystallogr.* **1985**, B41, 244– 247.

[18] Attfield, J. P. *Solid State Sci.* **2006**, 8, 861– 867.

[19] Rodriguez-Carvajal, J.; Bouree, F. *EPJ Web Conf.* **2012**, 22, 00010.

[20] Yeomans, J. M. *Statistical Mechanics of Phase Transitions*; Oxford University Press: Great Britain, **1993**.

[21] Pederzolli, D. R.; Attfield, J. P. *J. Solid State Chem.* **1998**, 136, 137– 140.

[22] Attfield, J. P.; Ferey, G. *J. Solid State Chem.* **1989**, 80, 112– 119.

[23] Haag, J. M.; Madsen, B. D.; Barnett, S. A.; Poeppelmeier, K. R. *Electrochem. Solid-State Lett.* **2008**, 11, B51– B53.

[24] Rodgers, J. A.; Williams, A. J.; Martinez-Lope, M. J.; Alonso, J. A.; Attfield, J. P. *Chem. Mater.* **2008**, 20, 4797– 4799.